

# Relative Photon-to-Carrier Efficiencies of Alternating Nanolayers of Zinc Phthalocyanine and C<sub>60</sub> Films Assessed by Time-Resolved Terahertz Spectroscopy

Okan Esenturk,<sup>\*,†,‡</sup> Joseph S. Melinger,<sup>§</sup> Paul A. Lane,<sup>||</sup> and Edwin J. Heilweil<sup>\*,‡</sup>

*Department of Chemistry and Biochemistry, University of Maryland, Building 091, College Park, Maryland 20742, Optical Technology Division, National Institute of Standards and Technology, Gaithersburg, Maryland 20899-8443, Electronics Science & Technology Division, Naval Research Laboratory, Washington, DC 20375-5320, Maryland 20899-844, and Optical Sciences Division, Naval Research Laboratory, Washington, DC 20375*

*Received: May 3, 2009; Revised Manuscript Received: July 26, 2009*

Multilayer and 1:1 blended films of zinc phthalocyanine (ZnPc) and buckminsterfullerene (C<sub>60</sub>) were investigated as model active layers for solar cells by time-resolved terahertz spectroscopy (TRTS). Relative photon-to-carrier efficiencies were determined from ultrafast decay dynamics of photogenerated carriers using 400 and 800 nm excitation for delay times up to 0.5 ns. The findings are in good agreement with reported solar-cell device measurements, and the results exhibit a near linear increase of the relative efficiencies with the interface number of multilayer films. The relative photon-to-carrier efficiencies of films composed of alternating layers with an individual layer thickness of less than 20 nm were higher than that of a 1:1 blended film. In contrast, 400 nm excitation of a C<sub>60</sub> only film initially yields a relatively strong THz signal that is followed by a rapid (picosecond) decay almost to its base value and results in a very low carrier density beyond a few picoseconds. For a given film thickness and optical density, our data suggest that the relative photon-to-carrier efficiency of multilayer films increases with increasing total interfacial area, emphasizing the importance of close proximity between the fullerene and phthalocyanine. These findings suggest that the highest photon-to-free-carrier efficiencies can be achieved by designing ultrathin films (having layers a few nanometers thick) with alternating multilayer structures to achieve high photon harvesting and charge separation to opposite layers.

## Introduction

Photovoltaics based on organic semiconductors continue to show much promise for solar energy conversion.<sup>1,2</sup> Such devices are based on thin films consisting of small organic molecules or, alternatively, large conjugated polymers. Thin organic films are attractive for a variety of reasons, including relatively easy solution processing, potential low cost, flexibility, and the ability to engineer their physical properties. In the case of photovoltaic devices based on small organic molecules, power conversion efficiencies in the range of 3–4% may be obtained.<sup>3</sup> To further optimize the performance of organic-based photovoltaics, it will be important to refine our understanding of photocarrier dynamics in the active organic layer. Two properties of particular importance are photocarrier generation efficiency and carrier relaxation back to equilibrium.

A variety of device structures are often used to characterize the electrical properties of the active organic layer. However, such characterization within a device can be affected by the metal–organic contact and device geometry, making determination of the intrinsic properties difficult. An alternative technique for investigating intrinsic electrical properties of materials is based on using ultrashort terahertz (THz) pulses.<sup>4</sup> In this method, the electrical properties of the organic thin film are determined spectroscopically, which eliminates the need for electrical contacts with the organic material. The technique of time-resolved THz spectroscopy (TRTS) combines ultrashort

THz pulses and optical pulses in a pump–probe configuration.<sup>5</sup> Here, the THz pulse probes the transient photoconductivity induced by the optical pulse, resulting in the determination of the electronic transport properties with (sub-)picosecond time scale resolution. TRTS has been applied to the characterization of intrinsic electronic transport in a variety of inorganic and organic materials.<sup>6–11</sup>

Thin films consisting of zinc phthalocyanine (ZnPc) and buckminsterfullerene (C<sub>60</sub>) are promising active materials for organic photovoltaics, as well as model materials for the study of photocarrier dynamics. In this Article, we use TRTS to investigate the carrier dynamics of blended ZnPc:C<sub>60</sub> films and of nanometer-scale multilayer films having alternating ZnPc and C<sub>60</sub> layers. We compare picosecond time scale dynamics in the range 1–500 ps for a series of ZnPc:C<sub>60</sub> multilayer films, and a single blended film prepared as a 1:1 ratio of ZnPc:C<sub>60</sub> by weight. The multilayer films contain alternating ZnPc and C<sub>60</sub> layers, where the layer thickness is varied systematically between 5 and 40 nm. Our TRTS studies of these films focus on the role that the interfacial region between ZnPc and C<sub>60</sub> plays in photocarrier generation efficiency and subsequent carrier relaxation dynamics. The TRTS transients for both blended and multilayer films are complex, exhibiting several components with decay times ranging from approximately 1 ps to about 1 ns. The relative strengths of the different temporal components are observed to vary in a sensitive way with respect to the layer thickness for the multilayer films. We discuss how our results from measurements of carrier generation efficiency and carrier relaxation relate to recent achievements of power conversion efficiency for small molecule photovoltaic devices made from blended and multilayer organic films.

\* Corresponding author. E-mail: esenturk@umd.edu (O.E.); edwin.heilweil@nist.gov (E.J.H.).

<sup>†</sup> University of Maryland.

<sup>‡</sup> National Institute of Standards and Technology.

<sup>§</sup> Electronics Science & Technology Division, Naval Research Laboratory.

<sup>||</sup> Optical Sciences Division, Naval Research Laboratory.

**TABLE 1: Optical Densities (ODs) of the Investigated Films at 400 nm**

film	OD
5 nm (alternating)	1.1
10 nm (alternating)	1.4
20 nm (alternating)	0.9
40 nm (alternating)	1.1
1:1 blend	0.5
ZnPc (neat)	1.1
C <sub>60</sub> (neat)	2.6

## Experimental Section

**Film Syntheses and Characterization.** All chemicals were purchased from Sigma-Aldrich Inc.<sup>12</sup> and purified via consecutive vacuum train sublimation. The blended and multilayer films of ZnPc and C<sub>60</sub> were deposited from separate resistive heating furnaces at a rate of 2 Å/s under high vacuum ( $\sim 6 \times 10^{-5}$  Pa). All samples were deposited on amorphous quartz substrates that yield no detectable THz generation from UV irradiation. A quartz crystal thickness monitor was used to monitor the deposition rate and to estimate the total thicknesses ( $\sim 200$  nm) of the deposited films. The blended film was prepared by simultaneous deposition of ZnPc and C<sub>60</sub> at a 1:1 weight percent ratio. Multilayered film structures were formed by vapor deposition of alternating nanolayers of ZnPc or C<sub>60</sub>. The alternating layer thickness ranged from 5 to 40 nm.

TRTS signal magnitudes are scaled with respect to the optical densities (OD) of each film because films with higher OD result in correspondingly larger differential THz transmission signals. Optical densities (at 400 nm) of the measured films are given in Table 1. UV absorption spectra of C<sub>60</sub>, ZnPc, 1:1 blend, and a 10 nm layered film are given in Figure 1 for comparison.

Figure 2a contains a schematic drawing of the alternating multilayer structured film deposited on an amorphous fused silica substrate examined by the TRTS measurement technique. The light and dark gray regions represent ZnPc and C<sub>60</sub> layers, respectively. This cartoon illustrates the interaction of the incident excitation light with the absorbing media at the photoactive region where carriers separate into opposing layers and diffuse in time (illustrated as hole, h<sup>+</sup>, and electron, e<sup>-</sup>, regions with contrasting colors inside the corresponding layers). Figure 2b depicts a possible mechanism for charge separation via optical excitation of ZnPc and electron transfer to C<sub>60</sub> during the early time dynamics measured by TRTS.

**Time-Resolved THz Spectrometer.** Details concerning the Ti:Sapphire kHz laser amplifier-based TRTS apparatus used in

this study were reported elsewhere.<sup>8</sup> The thin films were optically excited with 400 nm (3.1 eV, fluence of  $\sim 5 \times 10^{18}$  photons/m<sup>2</sup>), and similar 800 nm 60 fs pump pulses and interrogated with optically gated and synchronized time-delayed ultrafast THz probe pulses ( $\sim 0.5$  ps fwhm with center frequency at  $\sim 1$  THz). The strongest observed pump-induced modulation in the THz field is less than 1% of the peak transmitted THz field amplitude. The differential THz transmission time-dependent responses shown below were obtained by averaging between 40 and 120 individual TRTS transients (each sweep taking  $\sim 1$  min). Noise differences arise from averaging a different number of scans. The TRTS spectrometer is contained inside a plastic housing purged with dry and CO<sub>2</sub>-free air to minimize water vapor interference effects. Excitation average power of  $\sim 20$  mW (ca. 0.2 W/cm<sup>2</sup> or per pulse fluence of 8 GW/cm<sup>2</sup>) was well within the linear regime of power-dependent TRTS signals for these samples. A power dependence peak signal check was performed on a pure C<sub>60</sub> film (OD = 2.6) using up to 40 mW of excitation power, and a linear signal response was observed. We did not observe photo-oxidation or photobleaching of the films over the course of the measurements. However, minor nonreversible photodamage was observed for longer than 6 h of continuous photoexposure of the samples.

**Measurement Technique.** Figure 3a shows a typical time domain THz waveform, and Figure 3b shows the corresponding transient differential THz transmission signal (or  $\Delta T/T_0$ ) upon excitation of the film with respect to the pump-probe time delay. The differential transmission data are collected by monitoring the THz peak transmission amplitude (shown by the arrow in Figure 3a) as a function of the relative time delay between THz probe pulses and 400 nm pump pulses.

When the pump pulse impinges on the sample film, the material is photoexcited and carriers are generated. There is no detectable change in THz probe pulse amplitude before the 400 nm pump pulses arrives at the sample (time delay  $< 0$  ps), and the differential transmission is zero. A change in THz transmission is observed when the probe beam arrives at the same time as the pump beam excites ( $\sim 0$  ps) the sample or after the pump beam excitation (time delay  $> 0$  ps). The instrument has  $\sim 0.5$  ps time resolution (based on THz response measurements of a double-side polished silicon wafer). It is known that carrier generation in molecular-based semiconductor films occurs significantly faster ( $< 0.3$  ps)<sup>2,13-15</sup> than this instrumental time resolution. Therefore, the peak amplitude near zero delay between the pump and probe pulses (which is at  $\sim 1$  ps in Figure 4) is not directly proportional to the instantaneous generated carrier population but reflects an integrated amount detected by the system. The carrier population at the time of generation cannot be estimated from the response, but relative fractions of free-carrier population that exist at much later times ( $> 20$  ps in this case) can be used for relative photon-to-carrier efficiency comparisons between multilayered films. As the delay time changes, the differential THz transmission measures the free-carrier population evolution in time. This provides important information about the carrier recombination rates at early times along with the relative efficiency and carrier mobility of the materials.

At any given time delay, the measured differential THz transmission is proportional to the product of the effective mobility and carrier density, which in turn is proportional to the carrier generation efficiency (see ref 10 and references therein for more details). Because the multilayer films were composed of the same neat materials (ZnPc and C<sub>60</sub>), and only the individual layer thickness was changed, similar effective

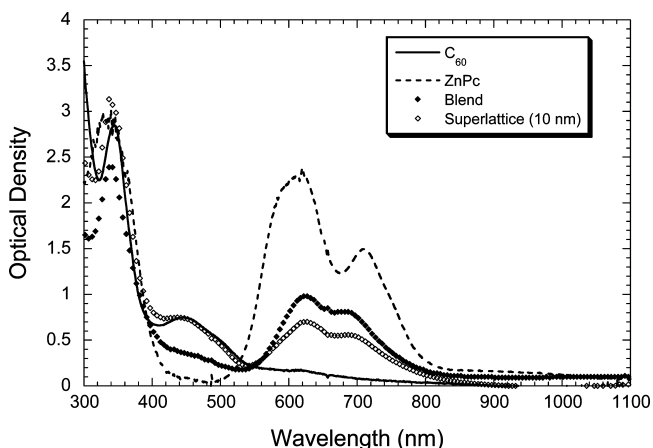


**Figure 1.** UV/vis absorption spectra of ZnPc, C<sub>60</sub>, 1:1 blend films, and a 10 nm alternating layered film.

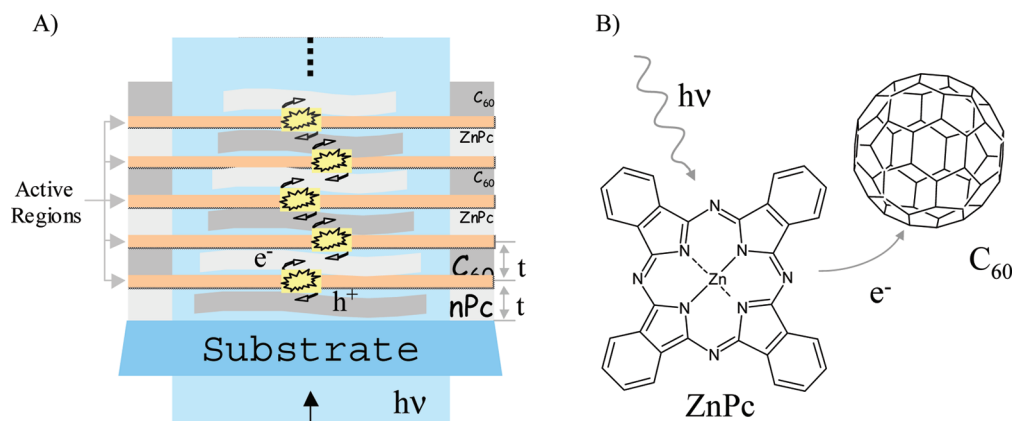


**Figure 2.** (a) A representative diagram of a multilayer film containing ZnPc and C<sub>60</sub>. The diagram also illustrates possible charge carrier generation at interfaces and its separation to the layers. Wavy arrows in the active regions represent carrier transfer to individual layers, and contrasting colors show isolated free carriers in the layers. Excitation and probing was conducted through the substrate. (b) A possible mechanism for the photoexcitation and charge transfer process of the ZnPc–C<sub>60</sub> system.

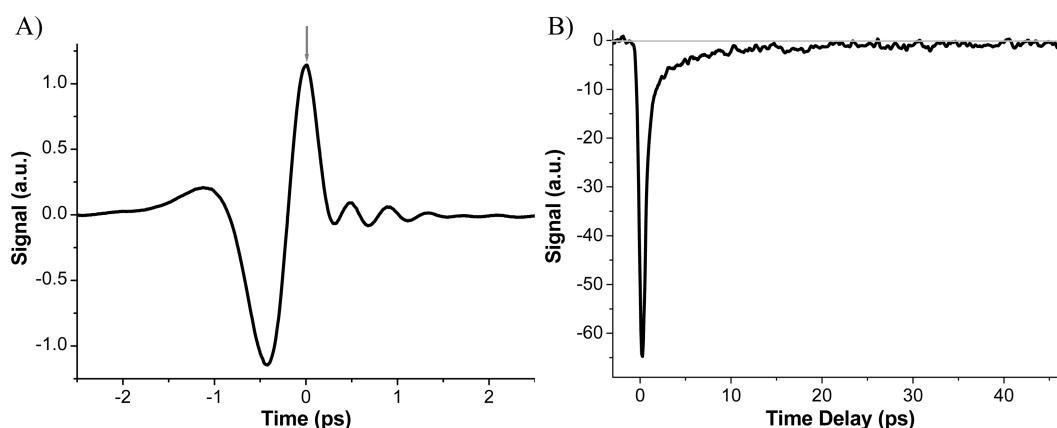


**Figure 3.** (a) A typical THz waveform showing the transmission of time domain THz waves passing through a sample (vapor-deposited C<sub>60</sub>). (b) Transient differential THz transmission data from the same C<sub>60</sub> sample.

mobilities were assumed for all of the films while the carrier concentration is assumed to be changing with the change in thickness or with the change in interfacial number (and interfacial area). Therefore, the comparison of differential THz transmission signals for films at a fixed delay time (that is >20 ps in these studies) directly compares the relative carrier density resulting from photoexcitation of the films. The relative decay rates and signal levels are used to evaluate the efficiencies of the multilayer films relative to each other.

## Results and Discussion

Results from early time (<50 ps) dynamics studies of the alternating multilayer films by TRTS using 400 and 800 nm excitation suggest two independent contributions to the charge carrier generation: in bulk media (mainly C<sub>60</sub>) and at the ZnPc/C<sub>60</sub> interface. Negligible charge generation of neat ZnPc film via excitation using both pump wavelengths supports a strong exciton binding energy as expected for small organic molecules.<sup>2,16–20</sup> Moreover, excitation of a pure C<sub>60</sub> film at 400 nm results mainly in very short-lived carriers. However, we find that the alternating nanolayer structures of ZnPc and C<sub>60</sub> result in long-lived carrier signals, and their amplitudes are proportional to the interfacial numbers of the films. These results suggest that generation of the long-lived carriers strongly depends on interfacial area between ZnPc and C<sub>60</sub> rather than the bulk content of the films.

**A. Differential Transmission Signals from Alternating Multilayer Films.** Figure 4 compares the measured transient differential THz transmissions of several alternating multilayer

films (of varying nanolayer thickness) and a 1:1 blended film of ZnPc and C<sub>60</sub> along with that of neat C<sub>60</sub> and neat ZnPc films. The data are corrected for OD variations at the 400 nm excitation wavelength because higher OD results in correspondingly higher signals (see Experimental Section for individual OD values and UV spectra of the films). The noise variations of the measured differential transmission data (in Figure 4) are due to differences in the number of averages and are significantly lower than the signal levels.

Prior to pump pulse arrival (time delay,  $t$ , < 1 ps) at the sample, no change in differential transmission is observed. This shows that only the carrier dynamics are observed in these measurements, and the dynamics are due to film photoexcitation with no instrumental contributions. Once the pump pulse arrives ( $t \approx 1$  ps), carriers are generated and their population dynamics evolves in time ( $t > 1$  ps, refers to the region beyond the peak transient and the corresponding decay data). Relatively strong initial responses (at  $t \approx 1$  ps) upon 400 nm excitation were observed for both the neat C<sub>60</sub> (green line) and the multilayer films. However, excitation of ZnPc resulted in a negligible signal response (gray line). The strong initial response is followed by a multicomponent decay as the carrier population decreases and evolves in time. The differential transmission response of the neat C<sub>60</sub> film exhibits an ultrafast decay after the initial growth. More than 90% of the carriers generated by the photoexcitation disappear within 5 ps.

The decay dynamics of the alternating multilayer films are significantly different from the neat C<sub>60</sub> film response, and the

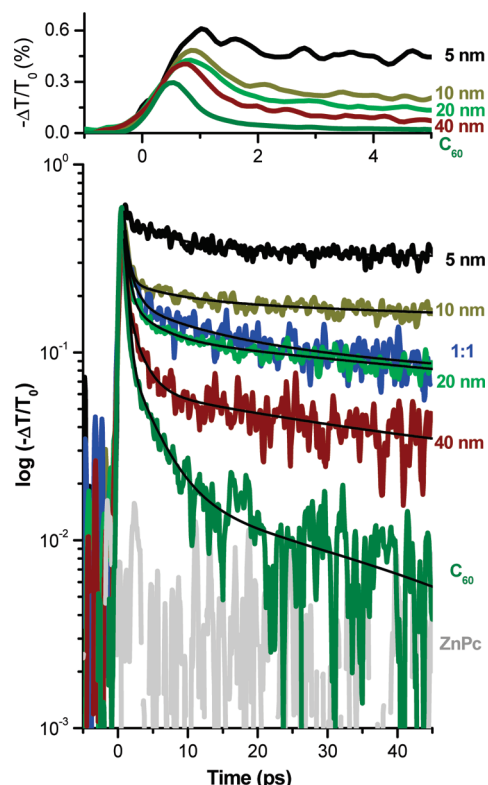


**Figure 4.** Transient differential transmission response for alternating multilayered films of ZnPc and C<sub>60</sub> with various layer thickness, a 1:1 blend ZnPc:C<sub>60</sub> film, and neat C<sub>60</sub> and ZnPc films. The data are corrected for OD variations of the samples at 400 nm. (Top) Enlarged data between  $-1$  to  $10$  ps for multilayer films and neat C<sub>60</sub> film to demonstrate the increase in peak amplitude as the layer thickness decreases. The neat C<sub>60</sub> signal intensity is divided by 2 to correct for the multilayer film C<sub>60</sub> content (50%). (Bottom) Differential transmission data showing the decay dynamics of photogenerated carriers at early times ( $<50$  ps) plotted in logarithm scale to illustrate its multiexponential behavior.

TRTS signal increases in amplitude as the alternating layer thickness decreases.<sup>21</sup> Figure 4 also shows the multiexponential fit (thin solid lines) to the decay dynamics observed for the alternating multilayer films and neat C<sub>60</sub> film. The fitting parameters for a two exponential fit to the data are given in Table 2. The initial ultrafast decay rate ( $1/t_1$ ) associated with the multilayer films ( $\sim 1$  to  $3.5$  ps) is similar to that of the neat C<sub>60</sub> film with a lifetime ( $t_1$ ) of  $\sim 0.7$  ps, which is possibly limited by the instrument response. However, beyond about 2 ps, the multilayer films show a strong enhancement of the longer lived response as compared to the neat C<sub>60</sub> film. The limiting  $t_2$  time constants of the alternating multilayer films show decreasing decay rates for the carriers as the individual alternating layer thickness decreased from 40 to 5 nm. The slowest overall decay was observed for the multilayer film with 10 nm alternating layer thickness, but the highest population of long-lived carriers at later delay times ( $t > 20$  ps) occurs for the 5 nm layered sample. The large error bars for the extracted  $t_2$  time constant predominantly arise from the restricted time delay range investigated ( $t < 50$  ps) and noise levels. However, much longer relaxation times of more than 100 ps are observed for the long-lived carriers, and this finding will be discussed in the following section.

The reduction in decay rate as the layer thickness decreases may result from elimination of charge trapping and/or fast recombination sites that enable the carriers to reach the interface in the shortest distance from the bulk regions of the films. The

observed slowing in the decay rate may also result from increasing secondary charge generation contribution as the layer thickness decreases. The second possibility may dominate because: (1) the total interfacial area increases as the layer thickness decreases (while the total film thickness is approximately constant) in these multilayered films, which enables higher interface assisted charge generation; and (2) there is an increase in the peak amplitude and  $\sim 200$  fs shift in the peak position to later time as the layer thickness decreases (Figure 4). One would not expect the peak amplitude to increase and shift in time if only more carriers were retained after the initial charge generation. The results from 800 nm excitation also support the notion that an increase in charge generation occurs as the layer thickness is decreased (see below).

Enhancement of exciton dissociation to free carriers by the presence of an interface is a well-known phenomenon,<sup>17,22,23</sup> and this situation may be responsible for the observed increase in the peak amplitude and shift in the peak position as the layer thickness decreases or as the interface number increases for the alternating multilayer films. However, identifying which of the ZnPc and C<sub>60</sub> excitons is the dominant component to the observed effect remains an open question. In an attempt to identify the contribution from ZnPc exciton dissociation to the observed signals, we studied the response of the nanolayer films using 800 nm excitation (Figure 5). At 800 nm, absorption by C<sub>60</sub> is relatively small as compared to that of ZnPc (see Figure 2). High power ( $>40$  mW) excitation of the layered films resulted in a similar response (not shown) to direct 400 nm excitation, possibly due to two-photon absorption by C<sub>60</sub> in the multilayer films. The two-photon excitation of the C<sub>60</sub> component of the film is also monitored by excitation of neat C<sub>60</sub> film with 800 nm pulses using similar power (see black line in Figure 5). For excitation powers  $\leq 20$  mW, 800 nm excitation of both neat ZnPc and neat C<sub>60</sub> films resulted in negligible transient signal levels, suggesting that the observed TRTS signal for nanolayered films using 800 nm excitation arises from charge transfer from ZnPc to C<sub>60</sub>. This result agrees with the findings by Lloyd et al. from a CuPc/C<sub>60</sub> photocurrent study where it was shown that electron transfer from CuPc to C<sub>60</sub> is the main process as compared to energy transfer in the region where CuPc dominantly absorbs ( $>600$  nm).<sup>24</sup> However, we cannot rule out the possibility that generation of free carriers may occur by excitation of either ZnPc or C<sub>60</sub> because 800 nm absorption of C<sub>60</sub> molecules is not zero and weak absorption may still result in exciton dissociation aided by an interface.<sup>25</sup> The 10 nm alternating multilayer film TRTS response using 400 and 800 nm excitation is presented in Figure 5 (all other multilayer films exhibited a similar response). The transient data are corrected for excitation photon number and OD differences. The initially strong peak response (at  $t \approx 1$  ps) seen in the differential transmission signal via 400 nm excitation was not observed with 800 nm excitation. This observation confirms that the peak and rapid decay observed in the differential transmission response of the multilayered films via 400 nm excitation is dominated by the bulk C<sub>60</sub> response, especially for thick layered films. In addition, the decay dynamics resulting from using either 400 or 800 nm excitation of the multilayer films are very similar beyond the ultrafast decay of the bulk C<sub>60</sub> component ( $>10$  ps).

In summary, our measurements suggest that the  $t \approx 0$  peak response and the initial fast transient signal decay observed in these films using 400 nm excitation are dominated by the C<sub>60</sub> layers of the films, especially for the films with thick alternating layers (such as  $>10$  nm). The TRTS signal response from the alternating multilayered films also suggests there is a growing

**TABLE 2: Biexponential<sup>a</sup> Fit Parameters of the Multilayer Films and neat C<sub>60</sub> Film**

sample	A <sub>1</sub> (au)	t <sub>1</sub> (ps)	A <sub>2</sub> (au)	t <sub>2</sub> (ps)	R <sup>2</sup>
5 nm	0.90 ± 0.07	0.80 ± 0.04	0.21 ± 0.01	157 ± 6	0.88
10 nm	(9.9 ± 0.4) × 10 <sup>-6</sup>	3.5 ± 0.3	(1.71 ± 0.02) × 10 <sup>-5</sup>	218 ± 14	0.88
20 nm	(2.5 ± 0.2) × 10 <sup>-5</sup>	1.05 ± 0.06	(8.24 ± 0.07) × 10 <sup>-6</sup>	205 ± 13	0.82
40 nm	(2.2 ± 0.1) × 10 <sup>-5</sup>	1.45 ± 0.07	(2.2 ± 0.1) × 10 <sup>-6</sup>	103 ± 17	0.83
blend	(2.00 ± 0.03) × 10 <sup>-5</sup>	1.77 ± 0.03	(6.41 ± 0.06) × 10 <sup>-5</sup>	79 ± 2	0.98
C <sub>60</sub>	(7.9 ± 0.5) × 10 <sup>-5</sup>	0.65 ± 0.12	(1.1 ± 0.1) × 10 <sup>-6</sup>	44 ± 12	0.95

<sup>a</sup> The data are fit to  $y = A_1 \exp(-(x - x_0)/t_1) + A_2 \exp(-(x - x_0)/t_2)$  after subtracting the long-time nearly constant offset.

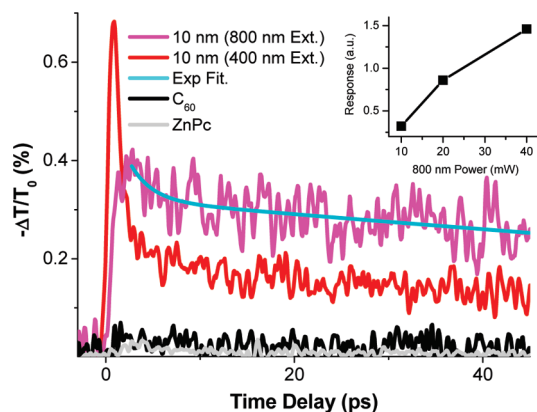


**Figure 5.** Differential THz transmission of an alternating multilayer ZnPc/C<sub>60</sub> film with 10 nm individual layer thickness, a neat ZnPc film, and a neat C<sub>60</sub> film. The films were excited with approximately 20 μJ of 400 and 800 nm pump pulses with a 2 mm beam diameter (ca. 8 GW/cm<sup>2</sup>). Data are corrected for film OD and photon number differences, and the signal decay response for 800 nm excitation fit to a double-exponential decay after subtracting the long time offset (see text). The inset shows the power dependence of the peak TRTS signal of the multilayer film using 800 nm excitation.

contribution from an interfacial charge generation mechanism that was also observed using 800 nm excitation. The increasing secondary (interface assisted) charge generation contribution explains the increase in peak amplitude and shift in peak position as the alternating ZnPc and C<sub>60</sub> layer thickness decreases for the data collected for 400 nm excitation of these alternating multilayer films. Although the observed two carrier generation contributions to the TRTS signal (one occurring within the bulk C<sub>60</sub> and the other at the interface of the alternating ZnPc and C<sub>60</sub> layers) occur roughly within the same time frame, the results suggest that the two processes are effectively independent of each other provided that the layer thickness is large relative to the effective width of the active region at the interfaces.

The free-carrier generation processes must depend on the chemical and physical properties of the materials, especially from C<sub>60</sub>, and their molecular interactions at the interface. With its highly localized conjugation, high ionization potential, and triply degenerate excited state, the C<sub>60</sub> molecule is a perfect candidate to be a many electron (up to six) acceptor.<sup>26,27</sup> However, the very fast decay response of the neat C<sub>60</sub> film also suggests that most of the carriers directly generated by excitation of C<sub>60</sub> do not travel far and rapidly recombine. Both the hole and the electron may delocalize inside the same molecule from which they are generated or a nearby C<sub>60</sub> molecule. This increases the probability of recombination and results in annihilation of most of the carriers within a few picoseconds, as observed in the data. However, free-electron carriers injected through the interface into the C<sub>60</sub> layer via direct photoexcitation of ZnPc or via hole transfer to the ZnPc layer leave freely migrating holes in the ZnPc layer and electrons in C<sub>60</sub> layer. In this scenario, the recombination lifetime is possibly limited by

tunneling of charges through the interface or by the annihilation of charges at the interface because back transfer is highly unlikely due to the built-in field at the interface by HOMO and LUMO of the ZnPc and the C<sub>60</sub>.<sup>13,19,28–30</sup>

Examination of a neat ZnPc film under identical measurement conditions as the mixed films showed that minimal carrier generation occurs by direct photoexcitation. The reported very low conductivity of neat ZnPc films<sup>31,32</sup> is a signature of low carrier population generation and low mobility of carriers in ZnPc as measured using TRTS. Our results strongly indicate that photogenerated ZnPc excitons do not dissociate into free charges within the measurement time frame unless C<sub>60</sub> is in very close proximity to the excited ZnPc molecule. This result suggests that ZnPc excitons are tightly bound and require strong neighboring electron-acceptor groups for dissociation to occur. These results agree with the reported high binding energies for ZnPc and other small organic films.<sup>2,32–35</sup> In addition, exciton diffusion in both the ZnPc and the C<sub>60</sub> bulk layers must be either very slow or nonexistent within the measured time frame (<50 ps) because the differential transmission signal level appears to depend linearly on the interfacial number, and significant deviation from this effect is not observed (see next section).

**B. Relative Photon-to-Carrier Efficiencies.** The amplitude of the differential transmission at delays well beyond the initial fast recombination times ( $t > 20$  ps in this study) is expected to be proportional to the relative carrier generation efficiencies of these model films, as discussed earlier in the Experimental Section. A direct comparison of the differential transmission amplitude at a long delay time, (i.e., 45 ps) to the photon-to-carrier efficiencies assumes similar effective mobilities for the films. Given that only the layer thickness is changing for each film and the total film thickness is kept approximately constant, this is a very reasonable assumption because the carrier mobility depends on the transport properties of bulk ZnPc and C<sub>60</sub> layers for the films. We acknowledge that this assumption may not hold as well for the thinnest (5 nm) layers due to possible changes in layer morphology near the interface, which in turn can alter the mobility.

The amplitude of the differential transmission data at 45 ps (see Figure 4), and hence the relative photon-to-carrier generation efficiencies of the films, increases as the layer thickness decreases. The 40 nm alternating layer film exhibits the lowest photoconversion efficiency, while the film with 5 nm alternating layers yields the highest free-carrier density. The increase observed in photon to long-lived carrier conversion as the alternating layers become thinner is due mainly to the increase in the interface number (or the total interfacial area of the films) rather than to the thickness of the layers. There is an inverse relation between the layer thickness and the number of interfaces in a film while the total film thickness is kept constant. For example, a 20 nm alternating multilayer film will have approximately twice the interface number relative to a film with 40 nm alternating layers, and will have one-half of the interface number as compared to a film with 10 nm alternating layers.

**TABLE 3: Ratio of Differential Transmission Signals at 45 ps (exp) and Ratios of Interface Numbers of Multilayer Films<sup>a</sup>**

ratio	exp	calc
5/10	2.0 ± 0.1	2.0
5/20	4.0 ± 0.2	4.1
5/40	9.0 ± 2.6	8.7
10/20	2.0 ± 0.1	2.0
10/40	4.5 ± 1.3	4.3
20/40	2.5 ± 0.8	2.1

<sup>a</sup> Exp. ratio =  $I_1/I_2$  at 45 ps time delay. Intensities ( $I_1$  and  $I_2$ ) are the average of 1 ps of data around 45 ps. Calc. ratio =  $n_{\text{int1}}/n_{\text{int2}}$  is the number of interface of film  $x$ . Errors are calculated from the standard deviations.

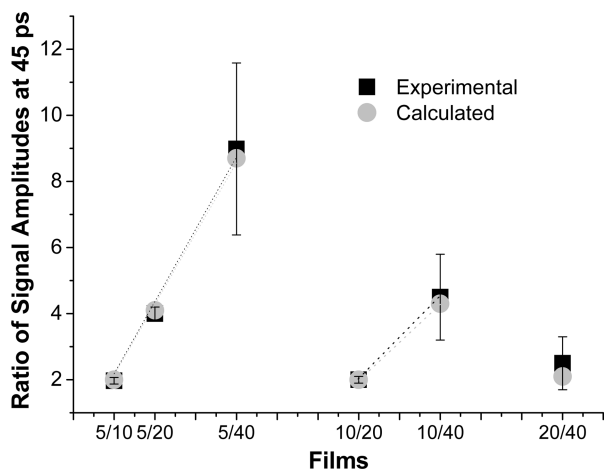


**Figure 6.** Comparison of the ratio of measured amplitudes at 45 ps and the ratio of calculated interface numbers for multilayer films with 5, 10, 20, and 40 nm individual layer thicknesses. Abcissa units such as 5/10 refer to the multilayer films and represent the TRTS signal amplitude at 45 ps of the 5 nm film divided by that of the 10 nm film, etc. See Table 3.

Similar interfacial number relations can be calculated for the films with other layer thicknesses.

Table 3 and Figure 6 compare the ratios of the TRTS signal amplitudes from the multilayer films measured at 45 ps to the ratios of interface numbers for these films. The calculated ratio of the interface number of one film to that of another (i.e., the ratio of the interface number of the film with 5 nm alternating layer to the interface number of the film with 10 nm alternating layers) shows a near linear correlation with the ratio of the TRTS signal amplitudes of the films (i.e., for 5 and 10 nm alternating layered films) measured at 45 ps. The near linear dependence of the TRTS signal (or relative efficiency) on the interfacial number suggests that there is a significant interfacial interaction between ZnPc and C<sub>60</sub> molecules and charge separation into the opposing molecular layers. In addition, such an interface number correlation can only be possible when there is no difference in the decay rates of the charge carriers generated at the interface (as seen in Figure 5) and when the interfacial generation and recombination processes are effectively independent of the C<sub>60</sub> carrier generation and recombination processes, as stated above. It is noteworthy that in a related device study examining 10 nm and larger alternating layers, Arbour et al. showed that the photocurrent increases linearly with the interfacial number.<sup>33</sup>

The correlation that persists for layer thicknesses down to 5 nm also suggests that the lowest thickness limit has not been reached for these multilayer films. The 5 nm thick layers of

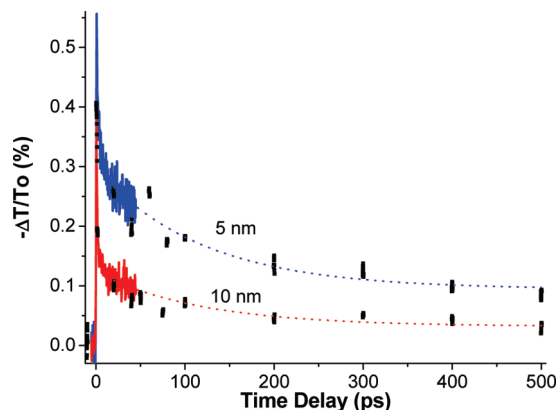


**Figure 7.** Differential THz transmission of 5 and 10 nm alternating multilayer films up to 0.5 ns time delay. The dotted lines are guides to emphasize that free carriers persist on the nanosecond or longer time scale.

ZnPc and C<sub>60</sub> are clearly sufficient to separate and keep charges apart from each other to achieve high photon-to-carrier efficiency. Given the molecular dimensions of C<sub>60</sub> (~0.75 nm diameter) and ZnPc (~1.5 nm length), 5 nm layers still provide multiple layers of molecules even if the ZnPc molecular plane is not completely parallel to the substrate.<sup>28,36,37</sup>

The results obtained for the 5 nm alternating multilayer film suggest that carrier generation and effective charge separation occur between the layers within a thin (<2.5 nm) active region at the interface. This small active region is on the order of molecular dimensions and suggests that excitation of ZnPc or C<sub>60</sub> results in either molecular (Frenkel)<sup>38</sup> or charge transfer excitons within the measurement time frame in these multilayer films.<sup>28</sup> One should note that this discussion is based on the time scale of our measurements (<1 ns) and may not correlate well with direct device or longer time measurements. However, the proposed active region thickness is on the same order of magnitude as that found in earlier reported device results, which also suggested a 5–10 nm active region at the interface<sup>2,33,39–41</sup> or a very small (6–10 nm) exciton diffusion length.<sup>2,16,39</sup> However, the active region thickness may also depend on the fabrication details of the layers, as suggested by Shevaleevskiy et al.<sup>42</sup>

A demonstration of possible correlation between the TRTS measurements to device measurements may be obtained for transient data extending out to 0.5 ns. Figure 7 shows measurements of the differential TRTS signals for the 5 and 10 nm alternating layered samples. The results show that the ratio of the differential transmission remains similar as the carrier population evolves in time and suggest that it may be maintained even after many nanoseconds (approaching the device measurement time scale).

The observed nanosecond or longer lifetime of carriers that are separated into opposing layers of multilayer films agrees with Arbour et al.'s conclusion<sup>28,33</sup> that highly ordered, pure molecular layers keep carriers apart from each other and minimize the recombination rate. However, our result disagrees with their proposed requirement of having a molecularly flat interface and that molecular interactions are not required for enhanced carrier separation. Our data show a strong correlation between the relative efficiencies to the interface number, hence, to the total interfacial area or molecular interactions. Our results further suggest that the films with well-separated layers and intermingled interfaces that increase the molecular interaction of the donor and acceptor molecules will increase the efficiency

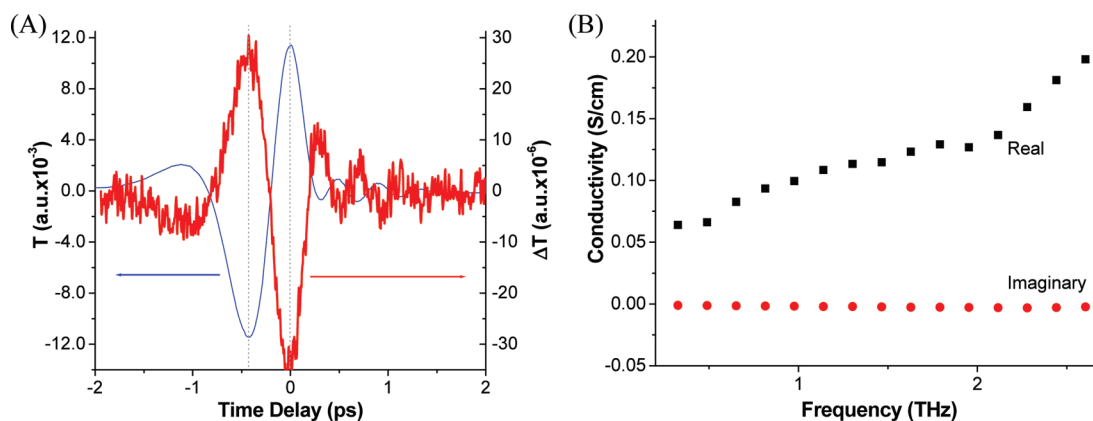


**Figure 8.** (a) Time domain spectra of reference and corresponding pump induced change in reference signal of THz transmission at 20 ps time delay of 5 nm film. (b) Corresponding frequency-dependent conductivities calculated from fast Fourier transforms of the measured time domain spectra.

of the device as a result of a better photon-to-carrier conversion in addition to having layered structure to separate the charges to different layers. Reported results of Hong et al. for devices that use nanometer thin layers between the conduction layers may be an example of this type of enhancement effect.<sup>16</sup>

**C. Multilayer versus Blended Film Comparison.** Figure 4 compares the transient differential signal amplitude for the nanolayered samples with the best blended film combination (1:1 by weight for ZnPc:C<sub>60</sub>). The best blend ratio (the film that yielded the largest signal at delay times near 50 ps) was determined from a study of six blend samples where the blending ratio changed from 0% to 100% mass fraction.<sup>43</sup> The layered and blend film results suggest that the 40 nm alternating layered film achieves a lower carrier generation efficiency than does the best blended film. This finding may also explain why thick layered film devices are inefficient as compared to a device containing only a blended film.<sup>3</sup> However, the 20 nm alternating layered film appears to approach the photon-to-carrier efficiency achieved by the best blended film, while the thinner layers yield significantly better performance in overall photon-to-carrier conversion.

One possible reason why the layered films appear to have higher conduction than the blended films is their ability to keep the charges separated. In blended films, the probability of charge–charge recombination is always high because the percolation path is not well-defined and depends on the blend film conditions (e.g., relative concentrations, isolated domains, inhomogeneities, etc.). However, in layered films with well-defined conduction paths and structure, carriers can be separated into the opposing layers so the recombination probability decreases. Such a separation of carriers is expected to improve the overall efficiency of the solar cell. There are already reports of using double and multilayered structures exhibiting enhanced performance over single layer blend heterojunction devices, and they could be considered as prototype devices employing alternating layered films.<sup>16,33,42,44–46</sup> However, further advancements in device engineering (e.g., film-to-electrode attachment design) are required to take advantage of the proposed efficiency observed via TRTS measurements on thin multilayer films.

**D. Frequency-Dependent Conductivities.** An important way to differentiate whether TRTS signals originate from free carriers as opposed to other sources such as excitons is by extracting the frequency-dependent conductivity. In general, semiconductor systems having a dominant real component of the conductivity indicate that free carriers are responsible for the measured signal.<sup>9</sup> Figure 8a shows absolute signal levels of

a reference THz waveform and the change in the transmitted THz waveform measured 20 ps after 400 nm photoexcitation of the 5 nm alternating multilayer film.

The overlap of the two waveforms shown in Figure 8 indicates that the measured differential THz transmission signal follows the reference single cycle THz pulse waveform but with opposite sign due to charge generation. The real and imaginary conductivities are calculated from the frequency-dependent phase and amplitude resulting from the fast Fourier transform of the reference THz waveform and the corresponding waveform for the pump-modulated sample (reference plus induced change).<sup>5</sup> Calculated real and imaginary conductivities for the 5 nm layered film are plotted in Figure 8b, and both the real and the imaginary conductivities exhibit a linear dependence with frequency. The significantly larger real conductivity (with approximately zero imaginary component) indicates that the measured TRTS signal is dominated by free carrier diffusion and exciton contributions are negligible.<sup>9</sup>

Conductivity models, including Drude–Smith, have been employed to describe free carrier conductivity of organic photoconducting systems measured with TRTS.<sup>6,7,9,10</sup> However, the fitting accuracy of the model requires a broader frequency bandwidth than that typically probed in a TRTS experiment (0.3–2.5 THz) up to a spectral region where the frequency-dependent conductivity deviates from the linear regime.<sup>11</sup> Unfortunately, our instrument is currently limited to an upper frequency of 2.8 THz so the nonlinear regime cannot be interrogated with our data. Extrapolation of the calculated real conductivity to 0 Hz estimates the DC conductivity of the samples measured by TRTS.<sup>6</sup> The 5 nm alternating film sample yields a DC conductivity of ~0.5 S/cm. This result is many orders of magnitude larger than the reported conductivity of neat ZnPc (<10<sup>-10</sup> S/cm) and neat C<sub>60</sub> (~4 × 10<sup>-8</sup> S/cm).<sup>32</sup> This result signifies the importance of having an electron acceptor group (C<sub>60</sub>) in close proximity to the donor (ZnPc) for efficient long-lived free carrier generation.

**E. Temperature-Dependent Conductivities.** Figure 9 shows the temperature dependence of the differential THz transmissions of the (a) 5 nm, (b) 10 nm, and (c) 40 nm alternating layered films and (d) 1:1 blend film of ZnPc/C<sub>60</sub>. The transient differential transmission for the neat C<sub>60</sub> film (not shown) did not exhibit any signal change at 78 K as compared to the room temperature measurement. This result is another indication that the photogeneration and subsequent dissociation of excitons to yield free charge carriers at early time occurs predominantly within the C<sub>60</sub> molecule itself, or the activation barrier for free-

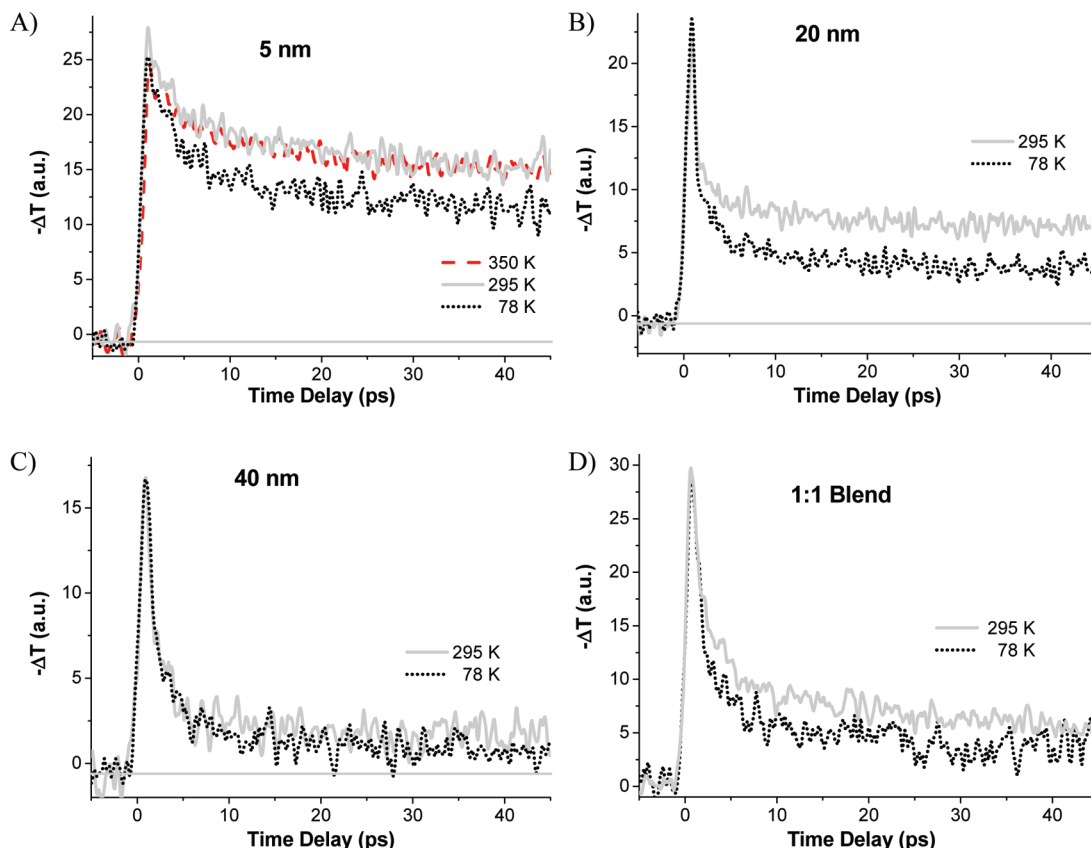


**Figure 9.** Differential transmissions of layered and blend films at room temperature and 78 K.

charge generation is very low for a process that involves a nearby  $C_{60}$  molecule. Measurements at lower temperatures (e.g., 10 K) may resolve mechanistic contributions involving secondary  $C_{60}$  acceptor molecules or direct free carrier generation in neat  $C_{60}$  films.

Differential transmission data of layered films at 78 K, however, show significantly faster decays at early time delays and similar decay rates after 10 ps as compared to those measured at 295 K. Because the neat  $C_{60}$  response is temperature independent, the measured change must be related to separation of the carriers generated at the interface. A faster decay suggests an increasing recombination rate for the carriers generated after the excitation. This may imply that the carriers are still within the Coulomb interaction range and may not be able to travel sufficiently far away from the generation site at lower temperatures, thus resulting in an increased probability for recombination relative to room temperature. However, once carriers travel sufficiently far away from the generation site, their diffusion does not seem to be affected by the lower temperature.

## Conclusions

In this investigation, we assessed the relative efficiencies of multilayered ZnPc/ $C_{60}$  thin films with nanometer thick alternating layers by monitoring the ultrafast decay dynamics of carriers with TRTS using 400 and 800 nm excitation wavelengths. The results showed increased photon-to-carrier efficiencies as the alternating layer thickness is decreased from 40 to 5 nm, and the relative efficiencies exhibit a linear dependence on the total interface number of the multilayer film rather than the thickness of the individual layers. Photoexcitation of neat ZnPc and multilayered films results in tightly bound excitons that require a strong interaction between ZnPc and  $C_{60}$  molecules to enable efficient free-carrier extraction. Photoexcitation of neat  $C_{60}$  with

400 nm pump pulses results in a relatively higher yield of photocarriers that recombine almost completely within the first 15 ps. Negligible long-lived carrier generation for neat  $C_{60}$  and neat ZnPc films explains why there are many orders of magnitude lower photoconductivities for neat component films as compared to those for layered and blended films of ZnPc and  $C_{60}$  observed in this study and related device measurements.

These TRTS layered film studies suggest there are two independent contributors to the carrier generation process. First, there is carrier generation within bulk  $C_{60}$  that does not result in a significant amount of long-lived carriers. Second, free carrier generation occurs at the interfaces (via exciton dissociation) of multilayer films within the active interaction regime of the ZnPc and  $C_{60}$  molecules. Our findings suggest that the latter may be the main driving force of conduction in these designs of solar cell devices.

The linear dependence of the relative efficiency to the interface number of multilayered films for layer thicknesses down to 5 nm suggests that photogenerated excitons are localized and experience very slow or possibly no diffusion within the experimental time frame of our measurements. In this view, applying synthetic methods to achieve very thin photoactive interfacial regions with thicknesses approaching a few nanometers should achieve the highest photon-to-carrier efficiencies for solar cell applications.

Temperature-dependent measurements also indicated that a slight increase of the early time recombination rate of the carriers occurs at lower temperature, but a similar longer-time decay rate (from free-carrier recombination) exists as compared to room temperature measurements. This increase in recombination rate may be correlated to the kinetic energies of the carriers or changes in film morphology.

Most noteworthy, this study demonstrates the strength of time-resolved THz probe measurements for assessing the free-carrier generation efficiencies of the photoactive layers in candidate solar cell materials. These relatively straightforward optical measurements suggest that TRTS will become a complementary technique to direct device measurements for the future characterization of new solar cell materials and device designs.

**Acknowledgment.** This work was partially supported by NIST Physics Laboratory internal Scientific and Technical Research Support (STRS) for E.J.H. and O.E. (Guest Researcher).

## References and Notes

- Gunes, S.; Neugebauer, H.; Sariciftci, N. S. *Chem. Rev.* **2007**, *107*, 1324.
- Peumans, P.; Yakimov, A.; Forrest, S. R. *J. Appl. Phys.* **2003**, *93*, 3693.
- Uchida, S.; Xue, J. G.; Rand, B. P.; Forrest, S. R. *Appl. Phys. Lett.* **2004**, *84*, 4218.
- Jeon, T.-I.; Grischkowsky, D. *Phys. Rev. Lett.* **1997**, *78*, 1106.
- Schmuttenmaer, C. A. *Chem. Rev.* **2004**, *104*, 1759.
- Ai, X.; Beard, M. C.; Knutsen, K. P.; Shaheen, S. E.; Rumbles, G.; Ellingson, R. J. *J. Phys. Chem. B* **2006**, *110*, 25462.
- Cunningham, P. D.; Hayden, L. M. *J. Phys. Chem. C* **2008**, *112*, 7928.
- Esenturk, O.; Melinger, J. S.; Heilweil, E. J. *J. Appl. Phys.* **2008**, *103*, 023102.
- Hendry, E.; Schins, J. M.; Candeias, L. P.; Siebbeles, L. D. A.; Bonn, M. *Phys. Rev. Lett.* **2004**, *92*, 196601.
- Ostroverkhova, O.; Cooke, D. G.; Shcherbyna, S.; Egerton, R. F.; Hegmann, F. A.; Tykwinski, R. R.; Anthony, J. E. *Phys. Rev. B* **2005**, *71*, 035204.
- Parkinson, P.; Lloyd-Hughes, J.; Johnston, M. B.; Herz, L. M. *Phys. Rev. B* **2008**, *78*, 115321.
- Certain commercial equipment, instruments, or materials are identified in this Article to adequately specify the experimental procedure. In no case does identification imply recommendation or endorsement by NIST, nor does it imply that the materials or equipment identified are necessarily the best available for the purpose.
- Brabec, C. J.; Sariciftci, N. S.; Hummelen, J. C. *Adv. Funct. Mater.* **2001**, *11*, 15.
- van Hal, P. A.; Janssen, R. A. J.; Lanzani, G.; Cerullo, G.; Zavelani-Rossi, M.; De Silvestri, S. *Chem. Phys. Lett.* **2001**, *345*, 33.
- Zerza, G.; Brabec, C. J.; Cerullo, G.; De Silvestri, S.; Sariciftci, N. S. *Synth. Met.* **2001**, *119*, 637.
- Hong, Z. R.; Maennig, B.; Lessmann, R.; Pfeiffer, M.; Leo, K.; Simon, P. *Appl. Phys. Lett.* **2007**, *90*, 203505.
- Gregg, B. A.; Hanna, M. C. *J. Appl. Phys.* **2003**, *93*, 3605.
- Hill, I. G.; Kahn, A.; Soos, Z. G.; Pascal Jr. *Chem. Phys. Lett.* **2000**, *327*, 181.
- Hoppe, H.; Sariciftci, N. S. *J. Mater. Res.* **2004**, *19*, 1924.
- Knupfer, M.; Peisert, H.; Schwieger, T. *Phys. Rev. B* **2001**, *65*, 033204.
- The fraction of the bulk  $C_{60}$  to the interfacial  $C_{60}$  decreases as the alternating layer thickness decreases and the interface number increases in these multilayer films. The subtraction of  $C_{60}$  contribution from the measured TRTS signal does not consider a change in the bulk  $C_{60}$  amount of the films. This will certainly cause differences in the calculated signals, especially for the first few picoseconds where the bulk  $C_{60}$  contribution is significant, as seen in the figure.
- Halls, J. J. M.; Walsh, C. A.; Greenham, N. C.; Marseglia, E. A.; Friend, R. H.; Moratti, S. C.; Holmes, A. B. *Nature* **2002**, *376*, 498.
- Yu, G.; Gao, J.; Hummelen, J. C.; Wudl, F.; Heeger, A. J. *Science* **1995**, *270*, 1789.
- Lloyd, M. T.; Lim, Y.-F.; Malliaras, G. G. *App. Phys. Lett.* **2008**, *92*, 143308.
- Investigations of layered film TRTS responses using tunable excitation pulses are underway to resolve the potential mechanism of charge creation.
- Koeppe, R.; Sariciftci, N. S. *Photochem. Photobiol. Sci.* **2006**, *5*, 1122.
- Fowler, P. W.; Ceulemans, A. *J. Phys. Chem.* **1995**, *99*, 508.
- Forrest, S. R. *Chem. Rev.* **1997**, *97*, 1793.
- Hiramoto, M.; Suezaki, M.; Yokoyama, M. *Chem. Lett.* **1990**, *19*, 327.
- Sato, Y.; Yamagishi, K.; Yamashita, M. *Opt. Rev.* **2005**, *12*, 324.
- Siebentritt, S.; Gunster, S.; Meissner, D. *Synth. Met.* **1991**, *41*, 1173.
- Walzer, K.; Maennig, B.; Pfeiffer, M.; Leo, K. *Chem. Rev.* **2007**, *107*, 1233.
- Arbour, C.; Armstrong, N. R.; Brina, R.; Collins, G.; Danziger, J.; Dodelet, J. P.; Lee, P.; Nebesny, K. W.; Pankow, J.; Waite, S. *Mol. Cryst. Liq. Cryst.* **1990**, *183*, 307.
- Peumans, P.; Bulovic, V.; Forrest, S. R. *Appl. Phys. Lett.* **2000**, *76*, 3855.
- Senthilarasu, S.; Sathyamoorthy, R.; Ascencio, J. A.; Lee, S.-H.; Hahn, Y. B. *J. Appl. Phys.* **2007**, *101*, 034111.
- Yim, S.; Heutz, S.; Jones, T. S. *Phys. Rev. B* **2003**, *67*, 165308.
- Sakurai, T.; Fukasawa, R.; Kawai, S.; Akimoto, K. *Jpn. J. Appl. Phys., Part 1* **2006**, *45*, 397.
- Dexheimer, S. L. Ultrafast Dynamics of Electronic and Vibrational Excitations in Fullerenes. In *Optical and Electronic Properties of Fullerenes and Fullerene-Based Materials*; Shinar, J., Varnedy, Z. V., Kafafi, Z. H., Eds.; Marcel Dekker Inc.: New York, 2000; p 21.
- Rostalski, J. R.; Meissner, D. *Sol. Energy Mater. Sol. Cells* **2000**, *63*, 37.
- Siebentritt, S.; Gunster, S.; Meissner, D. *Mol. Cryst. Liq. Cryst.* **1993**, *229*, 111.
- Kim, J. Y.; Bard, A. J. *Chem. Phys. Lett.* **2004**, *383*, 11.
- Shevaleevskiy, O.; Larina, L.; Myong, S. Y.; Lim, K. S. *J. Electrochem. Soc.* **2006**, *153*, A1.
- Esenturk, O.; Melinger, J. S.; Lane, P. A.; Heilweil, E. J. Photocarrier Dynamics of Organic Semiconductors from Ultrafast Carrier Dynamics Measured by Time-Resolved Terahertz Spectroscopy. In *Organic Thin Films for Photonics Applications*; Herman, W., Flom, S., Foulger, S., Eds.; American Chemical Society: Washington, DC, in press.
- Rand, B. P.; Genoe, J.; Heremans, P.; Poortmans, J. *Prog. Photovoltaics* **2007**, *15*, 659.
- Rand, B. P.; Peumans, P.; Forrest, S. R. *J. Appl. Phys.* **2004**, *96*, 7519.
- Yakimov, A.; Forrest, S. R. *Appl. Phys. Lett.* **2002**, *80*, 1667.